

Article

Insight on Atmospheric Hydrothermal Aging for Polyester and Polyimide Film Used in Dry-Type Reactor

Hao Lin, Jiang Guo, Xiang Huang * and Shengbao Jiang

China Electric Power Research Institute, Wuhan 430074, China

* Correspondence: huangxiang@epri.sgcc.com.cn

Abstract: The breakdown of the dry-type reactor induced by being exposed to moisture needs to be further explored. For this purpose, as the common insulating films in the dry-type reactor, PET and PI films were targeted to investigate the effects of atmospheric hydrothermal aging on the microstructure, thermal stability, and mechanical properties of the films. As the result of hydrothermal aging, the moisture-based thermal degradation obviously occurred on the surface of both PET and PI films, even at a low temperature. More defects and flaws can be observed on the surface of PET than that of PI film, which were responsible for decreasing the transmittance and tensile strength of films. According to the statistical analysis with a one-sample t test, the thermal stability of aged PET and PI films has no significant difference with raw films during the hydrothermal aging. Compared with thermal stress, the hydrolysis of ester linkage and the imide ring are the main factors of hydrothermal aging for PET and PI films, respectively. Improving the waterproof ability of PET and PI films can be effective to prevent deterioration of the interturn insulation performance of the dry-type reactor.

Keywords: hydrothermal aging; polymer film; dry-type reactor



Citation: Lin, H.; Guo, J.; Huang, X.; Jiang, S. Insight on Atmospheric Hydrothermal Aging for Polyester and Polyimide Film Used in Dry-Type Reactor. *Coatings* **2023**, *13*, 253. <https://doi.org/10.3390/coatings13020253>

Academic Editor:
Alexandra Muñoz-Bonilla

Received: 20 December 2022
Revised: 12 January 2023
Accepted: 17 January 2023
Published: 21 January 2023



Copyright: © 2023 by the authors. Licensee MDPI, Basel, Switzerland. This article is an open access article distributed under the terms and conditions of the Creative Commons Attribution (CC BY) license (<https://creativecommons.org/licenses/by/4.0/>).

1. Introduction

The dry-type reactor, as an important power compensation device, has been widely used in the power system because of its light weight, simple installation, low maintenance, and low cost [1,2]. However, the breakdown or even burning of dry-type reactors has been happening in operation for a long time. The possible operating failure of the dry-type reactor can be attributed to the insulation failure and local overheating, which depend on the aged insulation materials and unsuitable operating conditions [3–6]. For ensuring the safe and stable operation of the dry-type reactor, validating the quality and understanding the aging mechanism for insulation materials used in dry-type reactors is highly necessary.

In general, the dry-type reactor consists of several sealed packages of the coaxial winding. Moreover, the coaxial winding is wound parallel with single-strand electrical aluminum wire covered with the insulating film. The performance of the insulating film can directly affect the interturn and interlayer insulation of the dry-type reactor. Among various polymer insulation materials, polyimide (PI) has shown excellent performance in thermal stability, corrosion resistance, and insulation, and is applied in many special fields [7–10]. Some commercial PI films can be employed in a wide temperature range between -269 and 400 °C. Due to these remarkable advantages, PI film is regarded as a promising winding film for the interturn insulation of dry-type reactors. However, the high cost, as well as the complicated fabrication process, have limited expanding the application of PI film in comparison to other common insulation films, such as PET film [11,12]. The usage of inferior or counterfeit PI films such as dyed polyester (PET) film can bring a serious risk and endanger the running safety of various electric equipment. The structure, morphology, and thermal behavior of PI film have been characterized through a variety of analytical techniques, such as Raman spectroscopy, FTIR, electron microscopy, and thermogravimetric analysis [8,9]. Generally, the FTIR spectra of polyimide were used to distinguish from other

polymer films according to four characteristic peaks of the imide functional groups, at: 1778, 1378, 721, and 588 cm^{-1} [13]. Nonetheless, most of the characterization techniques rely on expensive instruments and specialized operation, which are not suitable for the rapid, on-site identification of PI films.

On the other hand, thermal aging was regarded as one of the main reasons for the deterioration of the interturn insulation of various polymer insulating films [14–19]. Many studies have been performed to study the influence of thermal aging on PI films at elevated temperatures [20–25]. These results indicated that some apparent changes, such as deviation of color and embrittlement, were induced by thermal oxidative degradation. Zhang et al. found that thermal aging at 300 °C in air resulted in the decrease of dielectric properties and breakdown strength of PI film [21]. Furthermore, thermal aging combined with other effects such as humidity, solar radiation, and stress can also hasten the degradation of polymer film, especially for the polymers prepared by condensation [26–29]. Aging induced by thermal stress can cause chain scission degradation, which firstly impairs the aromatic entities and finally, the carbonyls [28]. Some maintenance results showed that wetting can take place inside after the package of the faulted dry-type reactor is broken. Moisture in the package might be a factor causing the interturn insulation failure of the dry-type reactor. Braun et al. studied the hydrothermal degradation of PI films by the chemometric analysis of FTIR spectrometry and indicated that the hydrolysis of the imide groups does indeed proceed even at low temperatures [26]. Currently, the progress and mechanism of hydrothermal aging on PI film are still uncertain, and sometimes even controversial. Therefore, further studies need be explored to reveal the role of hydrothermal aging on various properties of PI insulating film under less extreme conditions.

In this study, PET, as another common insulating material, was chosen to be hydrothermally aged for comparison with PI film. The hydrothermal aging and its effect on PET and PI films was investigated based on the analysis of their microstructure, morphology, thermal behavior, and mechanical properties. The water adsorption kinetics on the two targeted films was studied to understand the hydrothermal aging progress and develop a relatively simple and effective method to validate the quality and performance of PET and PI films used in the dry-type reactor.

2. Experimental

2.1. Materials

In this study, commercially available PI and PET films with the thickness of 25 μm were purchased from Chenxi Corp. (Zhongshan, China). The structures of PET and PI films were polyethylene terephthalate and poly (pyromellitic dianhydride-co-4, 4-oxydianiline), respectively. The distilled water was purified by a Molelement 1815a system (Molecular Technology Instrument Co., Ltd., Shanghai, China). Anhydrous ethanol was of analytical purity and purchased from Sinopharm Group Chemical Reagents Co., Ltd (Shanghai, China).

2.2. Experimental Installation and Methods for Hydrothermal Aging

The operation temperature of the dry-type reactor cannot exceed 120 °C. According to a maintenance report, dampness or even some water can be found in the faulty dry-type reactor. The electrical aluminum wire covered with the insulating film might contact directly with water during the operating period of the dry-type reactor. Thus, an atmospheric accelerated hydrothermal aging condition was designed to simulate the interior condition of the dry-type reactor and study the moisture-based degradation of the insulating films. The setup of the hydrothermal aging device was composed of a thermostatic oil bath and a round-bottomed flask connected with the condensing pipe. Then, 300 mg of the targeted film was cut into several strips with the size of 20 \times 150 mm and immersed in 300 mL of distilled water at 90 °C. The film was taken out for analysis at various aging times. After aging treatment, the samples were cleaned by anhydrous ethanol and dried in an oven at 60 °C for 12 h before physical and chemical analysis.

2.3. Characterization Methods

The surface morphology of PET and PI films was examined using an optical microscope (OM; C3230BE, Shanghai Precision Instrument Co., Ltd.) and a field-emission scanning electron microscope (SEM; S4800, Hitachi). The magnifications of SEM were set as 5000 \times for each observation spot. Optical transmittance, T , and absorbance, A , in the wavelength range between 200 and 1200 nm were measured with an ultraviolet-visible near-infrared spectrometer (Lambda 750 S, PerkinElmer). Raman spectra were recorded on a laser microscopic confocal Raman spectrometer (DXR2 XI, Thermo Fisher Scientific) with a 532 nm wavelength laser. All ATR-FTIR spectra were recorded in transmittance mode using a Nicolet™ Fourier Transform Infrared (FTIR) spectrometer (NEXUS 6700, Thermo Fisher Scientific). Mechanical properties of PET and PI films were performed at room temperature on an HT-2040 universal tensile testing machine with 0.5 mm/min of the tensile speed in accordance with GB/T1040.3–2006. At least three tests were repeated for each type of material. The thermogravimetric (TG) analysis was carried out on the TGA system (TG209 F3, NETZSCH) at a heating rate of 10 °C min⁻¹ from room temperature to 800 °C under a nitrogen atmosphere.

3. Results and Discussion

3.1. Characterization of PET and PI Films with Aging Time

The surface morphology of raw and aged PET and PI films was explored by the SEM and OM techniques (Figure 1). The surfaces of raw PET and PI films were shown as smooth and flat via SEM images in Figure 2a,c. After hydrothermal aging for 32 days, obvious defects and micro-voids could be seen on the surfaces of aged PET and PI films (as shown Figure 2b,d). Moreover, the micro-void density on the surface of the PET film was much higher than that on the surface of PI film under the same aging time, which may be attributed to the fact that the physicochemical properties of PI film are better than those of PET film. Compared with the SEM images of the PI film aged by dry thermal stress at 300 °C [25], more defects and flaws could be observed on the aged PI film in the hydrothermal condition at 90 °C. In addition to the effect of temperature, moisture was indeed an important factor affecting the aging of the PI film. Interestingly, the change between the OM images of raw and aged films showed a consistent tendency with their SEM images. Although OM images cannot supply the elaborate surface information of the films, the OM technique can be applied for the quick and general assessment of the surface morphology of films due to its good accuracy, ease of operation, and relatively low cost.

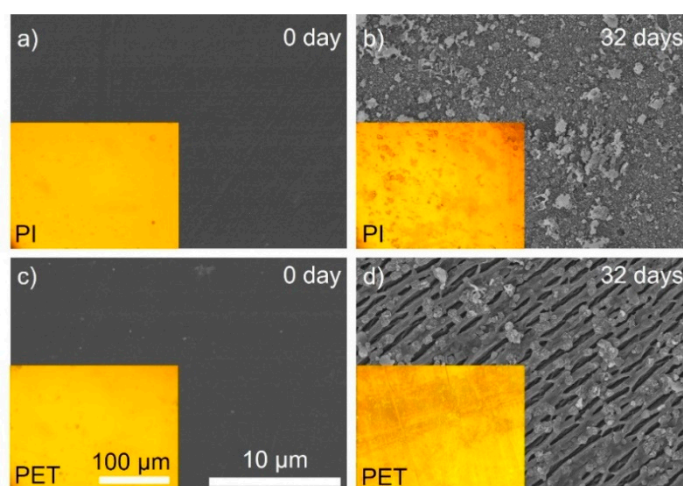


Figure 1. SEM images of (a,b) PET and (c,d) PI film surfaces: (a,c) raw films and (b,d) films aged for 32 days. The inserts in SEM images (a–d) are the corresponding optical micrographs of PET and PI films.

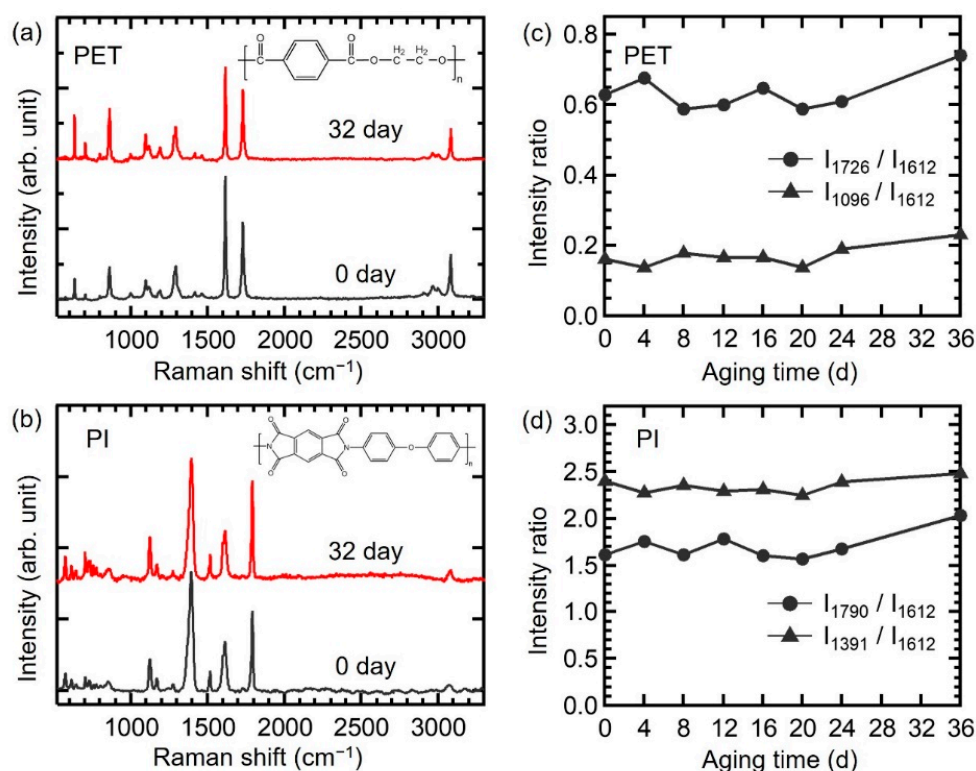


Figure 2. The Raman spectra of (a) raw PET and (b) PI films with their corresponding aging films. Influence of aging time on the relative intensity ratio of the functional groups on PET (c) and PI (d) films. The inserts in the Raman spectra are the corresponding structure diagrams of PET and PI films.

Compared with the conventional FTIR technique, Raman spectroscopy is suitable for studying the polymeric structures because of its high sensitivity for polymer materials and no requirement of any pretreatment. Thus, PET and PI films were analyzed by Raman spectrometry to investigate the influence of hydrothermal aging on the molecular structure. As shown in Figure 2a, the peak at 3082 cm⁻¹ was induced by the stretching vibration of C–H in PET film. The stretching vibration peak of the carbonyl group was at 1726 cm⁻¹. The stretching ring vibration of C=C in the benzene ring of PET was observed at 1612 cm⁻¹. Moreover, two bands at 1121 and 1096 cm⁻¹ confirmed the anti-stretching vibration of C–O in the glycol unit. The peaks below 900 cm⁻¹ were mainly attributed to the out-of-plane bending vibration of C–H in the benzene ring. Compared with the Raman spectrum of PET films, as shown in Figure 2b, Raman characteristic peaks of PI films at 1391 and 1123 cm⁻¹ were caused by C–N–C axial vibration and radial vibration, respectively. The vibration of C=O in the imide group caused the existence of a strong peak at 1790 cm⁻¹. The rigid aromatic ring led to a strong Raman peak at 1612 cm⁻¹, which was similar to that of the PET film. Therefore, the strong intensity at 1790 and 1391 cm⁻¹ in the Raman spectrum of PI can be used to identify PI from PET, which was similar to the previous reports [30]. Considering that the aromatic band showed very little variation in peak position and intensity by the fluence of hydrothermal aging, the Raman peak at 1612 cm⁻¹ was selected as the reference peak. The relative intensity ratios of bands at 1096 cm⁻¹ (C–O–C) and 1726 cm⁻¹ (C=O) were used to investigate the influence of hydrothermal aging on the PET film. Similarly, the relative intensity ratios of bands at 1391 cm⁻¹ (C–N–C) and 1790 cm⁻¹ (C=O) were used for PI film. As shown in Figure 2c,d, the relative intensity of C–O–C in PET and C–N–C in PI did not change much more during the investigated aging time. Likewise, the relative intensity of the carbonyl group on PET and PI films did not obviously change at the early stage of hydrothermal aging, and then it slightly increased after the aging for 32 days. The functional groups on the main skeletons of these two films possessed relatively high

stability during the hydrothermal aging process. In combination with the SEM results, it is speculated that the macromolecular chains on the surface of the two films may decompose first, while the main skeletons of the PET and PI films were not greatly affected by the combination of the thermal stress and hydrolysis.

To further investigate the influence of hydrothermal aging for the surface microstructure of the films, ATR-FTIR has been used to obtain the functional group information on the surface of the PET and PI films. As can be seen from Figure 3a, the peaks at 1718 cm^{-1} , 1409 cm^{-1} , and a pair of peaks with similar strength (1124 and 1253 cm^{-1}) were the characteristic peaks of the PET film caused by the stretching vibration of C=O, the skeleton vibration of the benzene ring (C=C), and the stretching vibration of C–O–C, respectively. To distinguish from PET film, the peak at 1772 cm^{-1} was chosen to represent the imide functional group of the PI film (Figure 3b). Moreover, the peaks at 1500 and 1337 cm^{-1} were the characteristic peaks of the PI film caused by the skeleton vibration of the aromatic ring (C=C) and the stretching vibration of C–N–C, respectively. After hydrothermal aging for 32 days, wide peaks at 3454 cm^{-1} (O–H stretches) and 3337 cm^{-1} (O–H and/or N–H stretches) could be observed in the ATR-FTIR spectrum of aged PET and PI films, respectively, confirming that the hydrolysis proceeded on the surfaces of both films. The intensity ratios of the two peaks were calculated and are shown in Table 1. The intensity ratios of these characteristic groups on the surfaces of PET and PI films clearly decreased after 32 days of hydrothermal aging, which may have resulted from the degradation and chain breaking that occurred on the surfaces of the films. These results further indicated that the ester linkage of PET and the imide ring of PI were indeed hydrolyzed on the surfaces of films in the hydrothermal environment at $90\text{ }^{\circ}\text{C}$, which was consistent with the reported results [26].

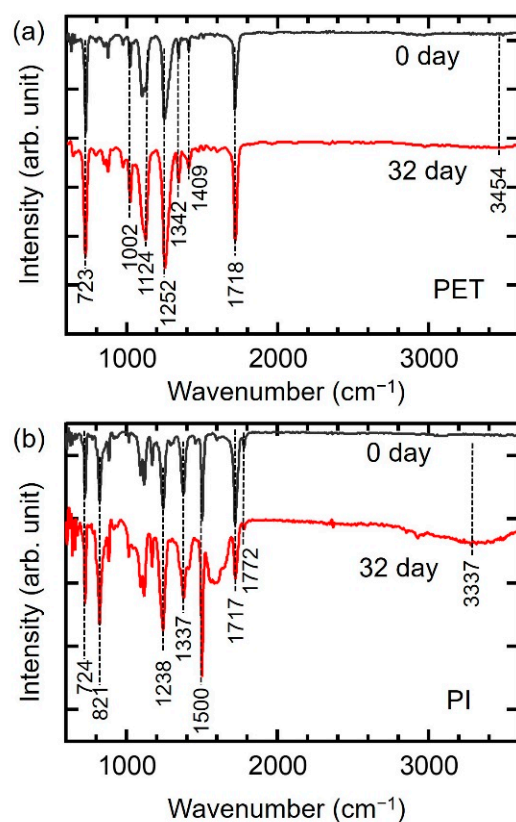
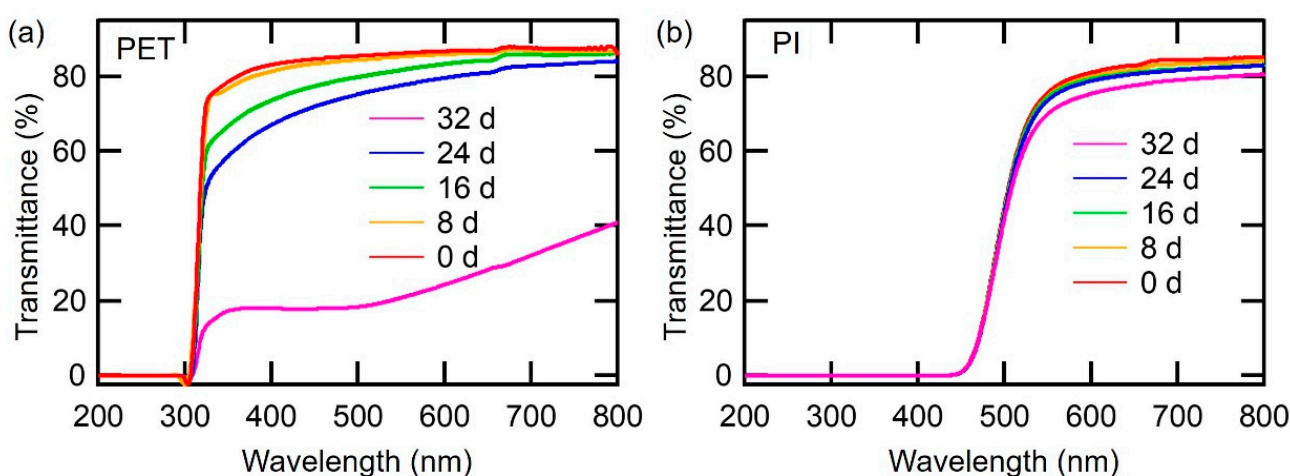


Figure 3. ATR-FTIR spectra of (a) raw PET and (b) raw PI films with their corresponding aging films.

Table 1. Influence of aging time on the ATR-FTIR group content of PET and PI films.

Hydrothermal Aging Time (days)	PET		PI	
	T_{1718}/T_{1409}	T_{1252}/T_{1409}	T_{1772}/T_{1500}	T_{1337}/T_{1500}
0	4.78	5.37	0.164	0.697
32	3.48	4.40	0.048	0.485

The change in the molecular structure and surface morphology can affect the optical absorption ability of PET and PI films. The absorption spectra for PET and PI films are shown in Figure 4. It could be found that the absorption edge of PET and PI films was about 320 and 540 nm, respectively. Both PET and PI films hardly absorbed light with a wavelength beyond 600 nm. The terephthalate groups in the structure of the PET film led to its absorption of ultraviolet light. Compared with the PET film, the macromolecular chain stacking of the PI film caused the extension of its visible light absorption. The transmission spectra of PET and PI film samples with different hydrothermal aging times were determined to study the aging process that occurred on the surfaces of the aged insulating films. The wavelength with a transmittance of 1% was defined as the cut-off wavelength. With increasing the hydrothermal aging time, no obvious variation of the cut-off wavelength was observed for PET and PI films. The transmittance at 600 nm of the PET film significantly decreased, more than that of the PI film. The transmittance of the PET film decreased by 71.8%, while that of the PI film decreased by 4.8%. Combined with the results of surface morphology, the micro-voids and flaws on the surface mainly resulted in decreased transmittance of the aged films.

**Figure 4.** UV-Vis transmission spectra of (a) PET and (b) PI films after aging for various times.

The thermal stability of the insulating film plays a crucial role in the normal operation of dry-type reactors with high-temperature processing. Thermal degradation analysis with the same heating rate was carried out for various aged PET and PI films. Figure 5 presents the TGA curves of PET and PI films aged at different times, including the initial decomposition temperature ($T_{5\%}$). The temperature of the maximum rate of decomposition (T_{max}) and the residual content (ω) at 800 °C are summarized in Table 2. As can be seen from Figure 5, all samples exhibited a similar one-step decomposition for both PET and PI films. The results listed in Table 2 show that $T_{5\%}$ and T_{max} of both insulating films slightly decreased with the increase of the hydrothermal aging time. The application of statistical analysis can more objectively evaluate the influence of hydrothermal aging on the thermal stability of PET and PI films. Therefore, the difference of $T_{5\%}$ and T_{max} between the raw films and the aged films was statistically analyzed with the one-sample t test by SPSS 23.0 software. The t test results showed that both $T_{5\%}$ and T_{max} of the two targeted films

aged at different times had no significant difference in comparison with those of the raw films ($p > 0.05$). Although thermal stress was regarded as the most important reason for deterioration of the insulation of polymer insulating films, the results indicated that the influence of hydrothermal aging on the thermal stability of PET and PI films was not the main factor of the interturn insulation failure of the dry-type reactor.

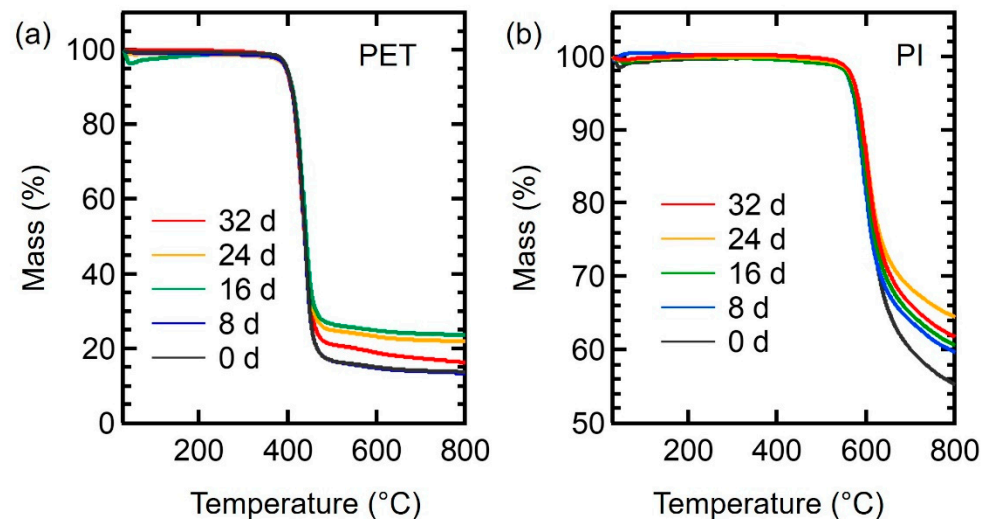


Figure 5. TGA curves of PET (a) and PI (b) films with various aging times.

Table 2. Results of TGA measurements for PET and PI films with different aging times ^a.

Aging Time (days)	PET			PI		
	T _{5%} (°C)	T _{max} (°C)	ω (%)	T _{5%} (°C)	T _{max} (°C)	ω (%)
0	397.5	437.9	13.77	577.4	603.5	55.37
8	396.1	437.4	13.50	572.4	596.6	60.71
16	398.1	437.6	23.72	579.0	601.5	64.57
24	395.2	436.9	22.04	578.7	603.5	61.83
32	395.3	434.8	16.43	570.2	595.7	59.76

^a T_{5%} (°C)—the corresponding temperature of 5% weight loss; T_{max} (°C)—the corresponding temperature of the maximum rate of decomposition; ω (%)—the weight residue of targeted films at 800 °C.

3.2. Mechanical Properties of Aged PET and PI Films

Figure 6 shows the influence of the hydrothermal aging time on the mechanical properties of PET and PI films. The tensile strength of neat PET and PI was 121 and 135 MPa, and the elongation was 20% and 43.2%, respectively. It can be seen that both the tensile strength and elongation for PET and PI films rapidly decreased as a result of the hydrothermal aging time. Especially after 32 days of aging, the elongation of the PET film sharply decreased and was close to 0%, indicating a significant reduction in the mechanical strength of the PET film. Compared with PET film, the influence of hydrothermal aging on the mechanical strength was smaller for the PI film. The decline of mechanical properties of the aged films was closely related to the density of the defects on the surface. The embrittlement of PET and PI films can lead to their fracture under internal stress, and then impair the interturn insulation, resulting in a short circuit of the dry-type reactor. Therefore, improving the water resistance and the mechanical properties of the insulation film can guarantee the longer operation of the dry-type reactor.

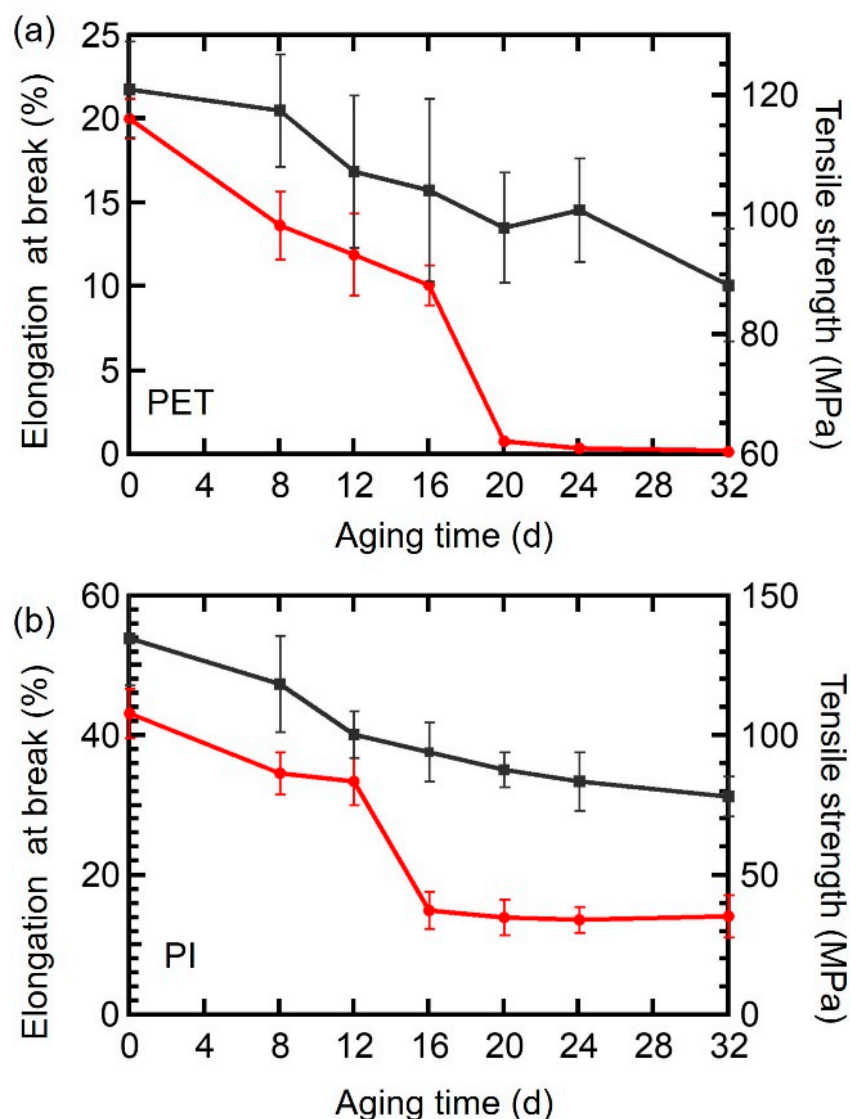


Figure 6. Influence of hydrothermal aging time on mechanical properties of PET (a) and PI (b) films.

3.3. Hygroscopicity Analysis of PET and PI Films

Changes in pH and EC values of the immersion solution with aging time were explored in Figure 7. It can be seen that the pH value of the PET immersion solution significantly decreased, more than that of the PI immersion solution. The pH value of the PET immersion solution became acidic after hydrothermal aging, which can be attributed to the carboxylic acid caused by the hydrolysis of the PET film. Due to the hydrolysates of the PI film having an amino group, the pH value of the PI immersion solution was near neutral. Moreover, the EC values of the PET immersion solution obviously increased in the later stage of the aging time compared with those of PI. During the hydrothermal aging process, PET and PI films can be hydrolyzed and release some charged organic molecules, which may deteriorate the interturn insulation of the dry-type reactor.

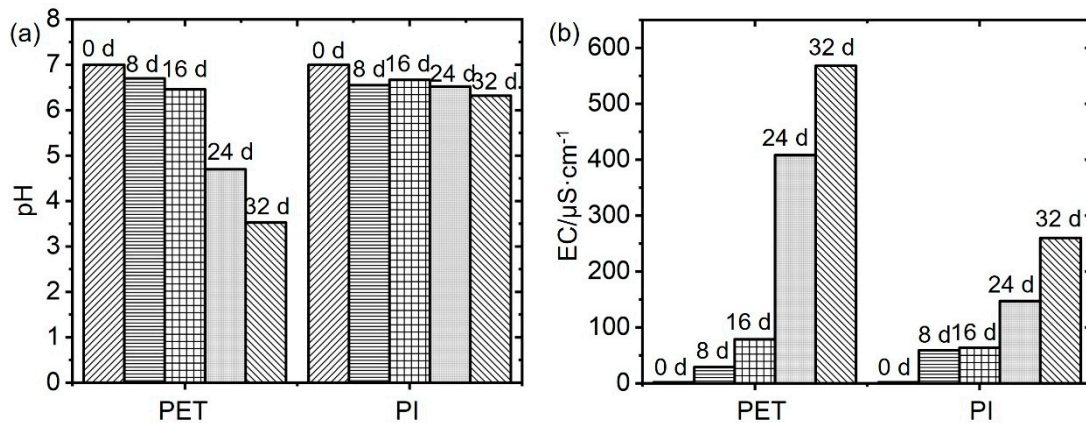


Figure 7. Influence of hydrothermal aging time on pH (a) and electronic conductivity (b) of immersion solutions of PET and PI films.

To understand the hydrothermal aging process, the water absorption curves of PET and PI films were studied in Figure 8. According to the experimental results, the water absorption processes of the two films were basically similar. The water absorption on these two films increased nonlinearly with the aging time, which rapidly increased within the initial 5 h and then slowly achieved an equilibrium at 120 h. Pseudo-first-order (Equation (1)), pseudo-second-order (Equation (2)), and Ritger–Peppas (Equation (3)) kinetic models were used to fit the experimental data for understanding the swelling kinetics and water diffusion behaviors on PET and PI films, as given below:

$$\ln(q_e - q_t) = \ln q_e - k_1 t \quad (1)$$

$$\frac{t}{q_t} = \frac{1}{k_2 q_e^2} + \frac{t}{q_e} \quad (2)$$

$$\ln F = \ln \frac{q_t}{q_e} = \ln k + n \ln t \quad (3)$$

where q_e (mg/g) and q_t (mg/g) correspond to the water adsorption capacity of the film at equilibrium and time t , respectively. The rate constant k_1 (h^{-1}) is determined from the slope of the linear plot of $\ln(q_e - q_t)$ against time t . k_2 ($\text{g} \cdot \text{mg}^{-1} \cdot \text{h}^{-1}$) is the rate constant of the pseudo-second-order adsorption, which can be calculated from the intercept and slope of the plot of (t/q_t) vs. time t . F is the fractional uptake at time t , k is a structure constant, and n is the swelling exponent, which determines the type of diffusion. The kinetic values of each model are listed in Table 3. The pseudo-second-order model ($R^2 > 0.999$) more accurately simulated the adsorption kinetics of water on the resulting films compared to other models. It was indicated that the adsorption process of water on both PET and PI films was affected mainly by chemisorption. The water diffusion mechanism was investigated through the Ritger–Peppas model [31]. The n values of the two films were fitted as near 0.5 within 5 h, implying that the diffusion mechanism of water on the films was apt to Fickian diffusion. The diffusion rate of water was much smaller than the relaxation rate of the film network. Subsequently, the n value became very small, being ascribed to water molecular-free diffusion on the films. Based on the above results, it can be deduced that the diffusion, adsorption, and reaction of water molecules preferentially proceeded in the amorphous region of the film, and it was difficult for water molecules to penetrate the crystalline region. After the amorphous region was slowly filled with water molecules, the absorption rate of water remained unchanged.

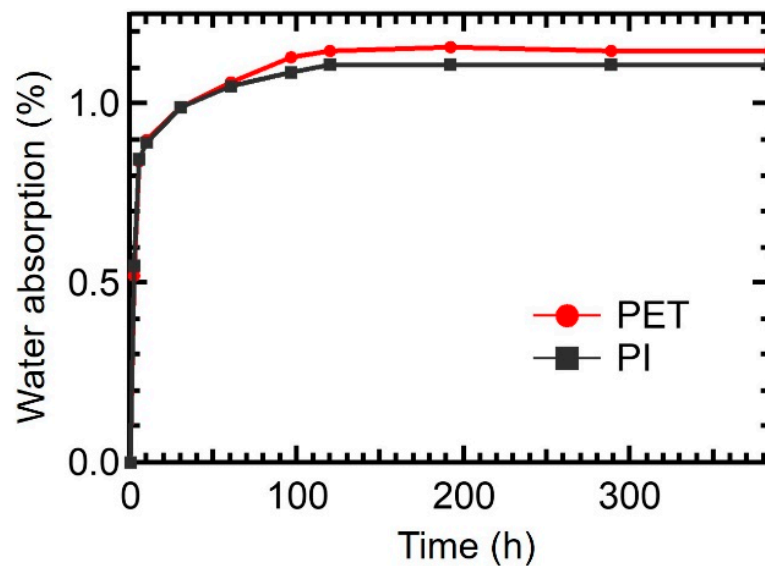


Figure 8. Water absorption curves of PET and PI films.

Table 3. Kinetic parameters of the water adsorption on PET and PI films.

Film	Pseudo-First-Order		Pseudo-Second-Order		Ritger-Peppas	
	k_1 (h^{-1})	R^2	k_2 ($\text{g}\cdot\text{mg}^{-1}\cdot\text{h}^{-1}$)	R^2	n	R^2
PET	0.0218	0.9517	0.165	0.9998	0.450 (<5 h) 0.099	0.9873 0.9907
PI	0.0217	0.9266	0.217	0.9999	0.452 (<5 h) 0.087	0.9989 0.9977

4. Conclusions

Although PI film possesses more excellent thermal and chemical stability than the PET film, the hydrothermal degradation clearly occurred on PI films. Many micro-voids and flaws were found to be formed on the surfaces of the two targeted films as a result of the hydrothermal aging, which were responsible for decreasing the transmittance and tensile strength of the films. According to the statistical analysis with the one-sample t-test, the thermal stability of the aged PET and PI films did not show a significant difference to the raw films during the hydrothermal aging at a low temperature. The hydrolysis of the ester linkage and the imide ring can be seen as the main factors responsible for the hydrothermal aging of PET and PI films, respectively. The adsorption process of water on PET and PI films was more accurately fitted with the pseudo-second-order model ($R^2 > 0.999$), implying that the mechanism of water adsorption is based on chemisorption. Therefore, humidity control and improving the waterproof ability of PI and PI films can be effective to prevent deterioration of the interturn insulation performance of the dry-type reactor.

Author Contributions: Conceptualization, H.L. and X.H.; investigation, J.G.; validation, J.G.; writing—original draft, H.L.; writing—review and editing, H.L., X.H. and S.J. All authors have read and agreed to the published version of the manuscript.

Funding: SGCC technology project “Research on main material selection method and reliability improvement technology of UHV converter main equipment under limit margin” (Program No. 5500-202055098A-0-0-00).

Institutional Review Board Statement: Not applicable.

Informed Consent Statement: Not applicable.

Data Availability Statement: Data generated or analyzed during this study are included in this published article.

Conflicts of Interest: The author declares no conflict of interest.

References

1. Enohnyaket, M.; Ekman, J. Analysis of Air-Core Reactors from DC to Very High Frequencies Using PEEC Models. *IEEE Trans. Power Deliv.* **2009**, *24*, 719–729. [[CrossRef](#)]
2. Rodriguez, D.J.; Alonso Orcajo, G.; Cano, J.M.; Norniella, J.G.; Vicente, A. Thermal Analysis of Dry-Type Air-Core Coils for the Optimization of Passive Filtering Systems. *Energies* **2020**, *13*, 4540. [[CrossRef](#)]
3. Zhao, Y.; Ma, X.; Yang, J. Online detection of inter-turn short circuit faults in dry-type air-core reactor. *Int. J. Appl. Electromagn. Mech.* **2012**, *39*, 443–449. [[CrossRef](#)]
4. Lei, X.; Xu, J.; Feng, B.; Chen, S. Lightning faults of DC dry-type air-core reactor in HVDC substation. *Energy Rep.* **2022**, *8*, 1378–1385. [[CrossRef](#)]
5. Nie, H.; Liu, X.; Wang, Y.; Yao, Y.; Gu, Z.; Zhang, C. Breaking Overvoltage of Dry-Type Air-Core Shunt Reactors and Its Cumulative Effect on the Interturn Insulation. *IEEE Access.* **2019**, *7*, 55707–55720. [[CrossRef](#)]
6. Silva Almeida, M.L.; Peres, L.M.; Silva, K.M. On applying an Enhanced Generalized Alpha Plane to shunt reactor protection. *Electr. Power Syst. Res.* **2022**, *212*, 108387. [[CrossRef](#)]
7. Zhang, Z.; Wu, Z.; Zhang, H.; Cheng, Y.; Ren, H. Analysis of Influence of Insulating Resin Paint Film on Enameled Wire Properties Based on Molecular Simulation. *Coatings* **2022**, *12*, 1352. [[CrossRef](#)]
8. Ogbonna, V.E.; Popoola, A.P.I.; Popoola, O.M.; Adeosun, S.O. Recent progress on improving the mechanical, thermal and electrical conductivity properties of polyimide matrix composites from nanofillers perspective for technological applications. *J. Polym. Eng.* **2021**, *41*, 768–787. [[CrossRef](#)]
9. Kausar, A. Progression from Polyimide to Polyimide Composite in Proton-Exchange Membrane Fuel Cell: A Review. *Polym. Plast. Technol. Eng.* **2017**, *56*, 1375–1390. [[CrossRef](#)]
10. Zhang, M.; Niu, H.; Wu, D. Polyimide Fibers with High Strength and High Modulus: Preparation, Structures, Properties, and Applications. *Macromol. Rapid Commun.* **2018**, *39*, e1800141. [[CrossRef](#)]
11. Lin, B.; Li, C.; Chen, F.; Liu, C. Continuous Blown Film Preparation of High Starch Content Composite Films with High Ultraviolet Aging Resistance and Excellent Mechanical Properties. *Polymers* **2021**, *13*, 3813. [[CrossRef](#)] [[PubMed](#)]
12. Tapaswi, P.K.; Ha, C.-S. Recent Trends on Transparent Colorless Polyimides with Balanced Thermal and Optical Properties: Design and Synthesis. *Macromol. Chem. Phys.* **2019**, *220*, 1800313. [[CrossRef](#)]
13. Dolez, P.I.; Tomer, N.S.; Malajati, Y. A quantitative method to compare the effect of thermal aging on the mechanical performance of fire protective fabrics. *J. Appl. Polym. Sci.* **2019**, *136*, 47045. [[CrossRef](#)]
14. Panowicz, R.; Konarzewski, M.; Durejko, T.; Szala, M.; Lazinska, M.; Czerwinska, M.; Prasula, P. Properties of Polyethylene Terephthalate (PET) after Thermo-Oxidative Aging. *Materials* **2021**, *14*, 3833. [[CrossRef](#)]
15. Oh, J.-H.; Park, C.H. Robust Fluorine-Free Superhydrophobic PET Fabric Using Alkaline Hydrolysis and Thermal Hydrophobic Aging Process. *Macromol. Mater. Eng.* **2018**, *303*, 1700673. [[CrossRef](#)]
16. Zuo, P.; Fitoussi, J.; Shirinbayan, M.; Bakir, F.; Tcharkhtchi, A. Thermal aging effects on overall mechanical behavior of short glass fiber-reinforced polyphenylene sulfide composites. *Polym. Eng. Sci.* **2019**, *59*, 765–772. [[CrossRef](#)]
17. Wang, H.; Zhu, Z.; Yuan, J.; Wang, H.; Wang, Z.; Yang, F.; Zhan, J.; Wang, L. A new recycling strategy for preparing flame retardants from polyphenylene sulfide waste textiles. *Compos. Commun.* **2021**, *27*, 100852. [[CrossRef](#)]
18. Liu, Q.; Li, J.; Cong, C.; Cui, H.; Xu, L.; Zhang, Y.; Meng, X.; Zhou, Q. Thermal and thermo-oxidative degradation of tetrafluoroethylene-propylene elastomer above 300 degrees C. *Polym. Degrad. Stab.* **2020**, *177*, 109180. [[CrossRef](#)]
19. Henri, V.; Dantras, E.; Lacabanne, C.; Dieudonne, A.; Koliatene, F. Thermal ageing of PTFE in the melted state: Influence of interdiffusion on the physicochemical structure. *Polym. Degrad. Stab.* **2020**, *171*, 109053. [[CrossRef](#)]
20. Zhuo, T.; Xin, B.; Chen, Z.; Xu, Y.; Zhou, X.; Yu, J. Enhanced thermal insulation properties of PI nanofiber membranes achieved by doping with SiO₂ nanoparticles. *Eur. Polym. J.* **2021**, *153*, 110489. [[CrossRef](#)]
21. Zhang, L.; Zhou, Y.; Mo, Y.; Zhou, Z.; Sha, Y.; Lu, Z.; Cheng, Z. Dielectric property and charge evolution behavior in thermally aged polyimide films. *Polym. Degrad. Stab.* **2018**, *156*, 292–300. [[CrossRef](#)]
22. Khazaka, R.; Locatelli, M.L.; Diahm, S.; Bidan, P. Effects of mechanical stresses, thickness and atmosphere on aging of polyimide thin films at high temperature. *Polym. Degrad. Stab.* **2013**, *98*, 361–367. [[CrossRef](#)]
23. Qin, S.; Tu, Y.; Wang, S.; Cheng, Y.; Chen, B.; Wang, C.; Zhang, Y. Accelerated Aging of Fast Thermal Cycle Effects on the behavior of Space Charge in Polyimide. *IEEE Trans. Dielectr. Electr. Insul.* **2017**, *24*, 3182–3190. [[CrossRef](#)]
24. Khazaka, R.; Locatelli, M.L.; Diahm, S.; Bidan, P. Endurance of Thin Insulation Polyimide Films for High-Temperature Power Module Applications. *IEEE Trans. Compon. Packag. Manuf. Technol.* **2013**, *3*, 811–817. [[CrossRef](#)]
25. Han, T.; Cavallini, A. Dielectric properties and partial discharge endurance of thermally aged nano-structured polyimide. *IEEE Electr. Insul. Mag.* **2020**, *36*, 39–46. [[CrossRef](#)]
26. Braun, C.A.; Nam, S.L.; de la Mata, A.P.; Harynuk, J.; Chung, H.J.; Dolez, P.I. Hydrothermal aging of polyimide film. *J. Appl. Polym. Sci.* **2022**, *139*, 1–11. [[CrossRef](#)]

27. Zhang, Y.; Miyauchi, M.; Nutt, S. Moisture absorption and hydrothermal aging of phenylethynyl-terminated pyromellitic dianhydride-type asymmetric polyimide and composites. *HIGH Perform. Polym.* **2019**, *31*, 1020–1029. [[CrossRef](#)]
28. Henri, V.; Dantras, E.; Lacabanne, C.; Koliatene, F.; Trebosc, C. Ageing of polyimide under thermal stress: Relaxational effects and charge transport. *Polym. Degrad. Stab.* **2021**, *186*, 109524. [[CrossRef](#)]
29. Cooper, R.; Ferguson, D.; Engelhart, D.P.; Hoffmann, R. Effects of Radiation Damage on Polyimide Resistivity. *J. Spacecr. Rockets* **2017**, *54*, 343–348. [[CrossRef](#)]
30. Kadiyala, A.K.; Sharma, M.; Bijwe, J. Exploration of thermoplastic polyimide as high temperature adhesive and understanding the interfacial chemistry using XPS, ToF-SIMS and Raman spectroscopy. *Mater. Design* **2016**, *109*, 622–633,1275. [[CrossRef](#)]
31. Ahmed, E.M.; Aggor, F.S.; Awad, A.M.; El-Aref, A.T. An innovative method for preparation of nanometal hydroxide superabsorbent hydrogel. *Carbohydr. Polym.* **2013**, *91*, 693–698. [[CrossRef](#)] [[PubMed](#)]

Disclaimer/Publisher's Note: The statements, opinions and data contained in all publications are solely those of the individual author(s) and contributor(s) and not of MDPI and/or the editor(s). MDPI and/or the editor(s) disclaim responsibility for any injury to people or property resulting from any ideas, methods, instructions or products referred to in the content.